IEEE Access
Multidisciplinary ⋮ Rapid Review ⋮ Open Access Journal

Received 27 December 2023, accepted 13 January 2024, date of publication 19 January 2024, date of current version 1 February 2024.

Digital Object Identifier 10.1109/ACCESS.2024.3356012

RESEARCH ARTICLE

Improved Relay Algorithm for Detection and Classification of Transmission Line Faults in Monopolar HVDC Transmission System Using Signum Function of Transient Energy

SOMA DEB[1], (Member, IEEE), SUMAN LATA[1], (Member, IEEE), VIKAS SINGH BHADORIA[2], SHUBHAM TIWARI[3], THEODOROS I. MARIS[4], VASILIKI VITA[5], AND GEORGIOS FOTIS[5]

[1]Department of Electrical Electronics and Communication Engineering, Sharda University, Greater Noida, Uttar Pradesh 201310, India
[2]IIC, Shri Vishwakarma Skill University, Palwal, Haryana 122003, India
[3]Department of Electrical and Electronics Engineering, ABES Engineering College, Ghaziabad, Uttar Pradesh 201009, India
[4]Core Department, National and Kapodistrian University of Athens (NKUA), Psahna, 34400 Euboea, Greece
[5]Department of Electrical and Electronics Engineering Educators, ASPETE—School of Pedagogical and Technological Education, 141 21 Heraklion, Greece

Corresponding author: Vikas Singh Bhadoria (vikasbhadoria@gmail.com)

This work was supported by the National and Kapodistrian University of Athens (NKUA).

ABSTRACT Based on the signum function (sign of magnitudes) of transient energy, this paper proposes a fault classification approach and algorithm for a monopolar HVDC system. The analytical study here shows that the signum function of variation in transient energy has a zero value individually at both ends on no-fault conditions. Moreover, the summation of the signum functions computed for internal DC faults is zero, whereas the same has a non-zero value for external AC faults. The performance of the proposed algorithm has been extensively evaluated by simulating faults on a CIGRE benchmark system for HVDC monopolar configuration using EMTDC/PSCAD software. Three locations of DC line fault, and AC fault at the two ends of the system have been considered for this evaluation. Five fault resistance values (0, 10, 100, 1000, and 2000 ohms) have been simulated for each fault location. The results conform with the theoretical analysis, and the fault classification by the algorithm is 100% accurate. The time taken to detect and classify a DC fault at the mid-point of the 800-km line is 1.5 ms, and that for line-end faults on the DC line is 3 ms for all values of fault resistance. These results show a marked improvement over those reported earlier in the literature using other techniques. A comparison table is given in the last section to corroborate it.

INDEX TERMS DC line fault, EMTDC/PSCAD, fault classification, fault detection, HVDC transmission line, signum function, transient energy.

I. INTRODUCTION

High voltage direct current (HVDC) transmission systems offer attractive advantages over high voltage alternating current (HVAC) transmission systems for long-distance and bulk power transmission [1], [2], [3]. India is expected to produce 500 GW of renewable energy by 2030 [4]. Renewable energy sources are typically far from the load centers [5], [6]. The role of HVDC technology in transmitting power to these load centers is crucial and cannot be overlooked. Total number of HVDC system installations worldwide has rapidly expanded in the past two decades. Line-commutated converter-based HVDC (LCC-HVDC) technology is best suited for transmitting bulk power over longer distances [7], [8].

As higher and higher powers are being transmitted on HVDC systems, their protection is becoming increasingly critical. The failure rate of the HVDC transmission line is much higher than any other component of the HVDC transmission system [9]. Also, most of the DC transmission line

The associate editor coordinating the review of this manuscript and approving it for publication was Huaqing Li.

faults are transient in nature. It is crucial to activate the DC line protection system only when a fault occurs within the DC line, rather than in the AC system or at the converters situated at either end, to prevent unwanted power outages [10], [11], [12]. This emphasizes the importance of precise fault identification in ensuring the HVDC transmission system operates steadily, securely, and reliably.

Conventional protection techniques used with HVDC transmission lines include protection based on the time derivative of the voltage and current signals, protection based on under-voltage, current differential protection schemes, and protection based on traveling waves [13].

Inrush current generated by the HVDC system converter transformer may cause unwanted triggering of the HVDC protection. This problem has been addressed in [14] using DC under-voltage protection with a current-restrained function. This approach differentiates between DC line faults and transformer inrush conditions based on the size and time length of 2nd harmonic component produced by the transformer inrush current.

A protection principle based on smoothing reactor voltage (SRV) is put forward in [15]. Since the polarity at the two ends of the line is equal on internal faults and opposite on external faults, the polarity of SRV is utilized to differentiate between internal and external faults. However, the selectivity and sensitivity of the proposed technique are reduced with an increase in fault resistance values and the length of the transmission line.

A fault detection technique employing the voltage change rate across the DC reactor has been given in [16]. DC reactors installed at the line terminals are among the significant parts of any HVDC transmission line and are used to limit the fault current. Also, there is no requirement for telecommunication infrastructure, no dependency on power flow direction, and insensitivity to variation in fault resistance. However, this method is computationally more complex and requires a higher sampling frequency based on the second derivative [17].

A reactive energy-based protection technique has been proposed in [18]. It is based on the direction of the reactive energy flow on both ends of the line. Here, the reactive energy is the integration of the reactive power over a specific time. Reactive energy calculations are done using the Hilbert transform. An internal fault on the DC line can be detected if the flow of reactive energy measured at both terminals is opposite. However, the protection sensitivity reduces with increasing fault resistance value. Also, the study has been made for fault resistance only up to 200 ohms.

Reference [19] proposed a differential current protection principle that eliminates the influence of capacitor current. The proposed protection scheme's sensitivity is much better than conventional differential current protection schemes. However, it is suitable only for backup protection principles.

References [20] and [21] proposed two more current differential protection schemes based on the compensation of distributed capacitive current. These schemes lack accuracy because of the ignorance of the distributed capacitance effect on the protection principle.

References [22] and [23] present methods for compensating distributed capacitive current using frequency-dependent and distributed parameter line models, respectively. However, because of their complicated calculations, sensitivity to noise, and parameter errors, these methods are challenging to apply in practical engineering applications.

Reference [24] proposes a new differential relay algorithm. The algorithm is implemented in PSCAD/EMTDC using a frequency-dependent phase model. The authors have validated the algorithm for fault resistance up to 1000 ohms. The obtained results show that the protection scheme's sensitivity reduces with increase in value of fault resistance. In [25], a unit protection algorithm is proposed based on the difference of current signals at both ends of the transmission line. The drawback of this method is that it can give oscillations, and the near-end or far-end faults cannot be identified correctly. Therefore, the protection scheme is found to have poor accuracy and poor reliability. A protection algorithm using the Pearson correlation coefficient of the current derivative has been proposed in [26]. Internal faults were differentiated from external faults using the current derivative of the DC filter. However, this protection algorithm is found to be susceptible to fault resistance values.

Based on the characteristics of the devices at the boundary of the HVDC transmission line, a protection scheme is proposed in [27]. However, the high sampling frequency requirement limits the protection algorithm's real-time application.

In [28] and [29], pilot safety schemes utilizing flying waves have been proposed. Still, their practical implementation poses challenges due to their sensitivity to fault transition impedance and the need for a high sampling frequency.

Reference [30] uses a bagged-tree ensemble-classifier (BTEC) protection technique for fault detection and classification in the DC transmission line. A massive set of data in the form of voltage and current signals is required from the simulation for training the protection algorithm. Moreover, the training data's amount greatly affects the protection algorithm's accuracy and reliability.

In [31] and [32], at specific tuned frequencies, the signs of surge impedance and inductive energy were obtained and used to build two pilot protection schemes, respectively. However, with the increased value of fault resistance, the protection scheme's reliability is reduced. Based on the difference in voltage values between the positive and negative poles of the HVDC system, a pilot protection principle is put forward [33].

In [34], a protection technique for fault detection and classification based on the measured value of surge impedance is put forward. Characteristics between amplitude versus frequency of the DC filter are utilized here for differentiating internal and external faults. However, the sensitivity of the

protection scheme is reduced with the increase in the value of fault resistance.

In [35], a pilot protection scheme is proposed based on the correlation of the current signal of the DC line and DC filter. Impedance versus frequency characteristics of the converter station's reactor, DC filter, and DC line are employed in [36] for fault identification and classification. The requirement of high sampling frequency limits the implementation of the protection algorithm.

With the fast advancement in the field of signal processing and sampling techniques working on high frequency, the reliability and applicability of the protection method based on travelling-wave have improved remarkably during the last few years in the field of HVDC protection [28], [37], [38]. However, lower accuracy and a decrease in relay sensitivity during high resistance faults, are the two significant shortcomings of these techniques [39], [40].

Reference [41] proposed another fault detection technique using the voltage across the DC reactor. The fault detection is based only on the DC reactor voltage at one of the terminals. However, the technique is effective only for faults with low resistance values and requires a special voltage transformer for the measurement of DC reactor voltage.

Based on the current measurements by optical current sensors mounted along the transmission line, reference [42] offers single-ended differential protection. This technology necessitates a large number of sensors and is uneconomical [43].

Thus, all the proposed techniques/schemes have either a poor sensitivity to high-resistance faults or a long operating time. In addition, in each case, the actual value of a specific variable (like current, reactive energy, or transient energy) is transmitted continuously from one end to the other of the protected line. Transmission of this value, being several digits in size, takes a long time and has some probability of communication error. This paper presents a protection approach that uses the signs (and not the actual values) of the variation in transient energy at both ends of the DC transmission line. Therefore, the data transmission time is reduced, and since the sign has only two values (+ and -), the chances of transmission error are minimal. Transient energy is defined here as the integral of the transient power over a specific time interval. In contrast, transient power is the product of the incremental values of voltage and current. Also, the effect of the distributed capacitance has been considered using the frequency-dependent phase model of the HVDC transmission line to obtain the current and voltage signals under transient conditions. Subsequently, a fault classification algorithm based on this approach is presented.

A detailed sensitivity study is presented in this paper, demonstrating that the protection scheme performs well with high as well as low resistance faults. The rest of the sections of this research paper are structured as follows. Section II outlines fault detection and classification principles. The fault classification algorithm is given in Section III, and its evaluation in Section V. Simulation and simulation results are shown in Section IV. The final section summarizes the entire research work. It compares the performance of the suggested technique/algorithm with those reported in the literature and is briefly discussed in this paper.

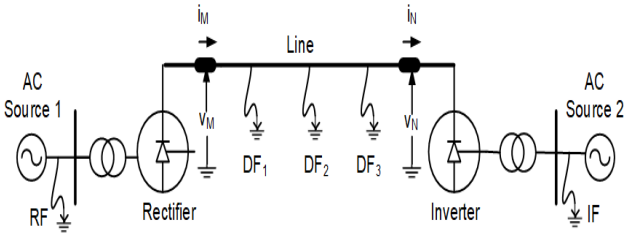

FIGURE 1. HVDC system and locations of faults.

II. FAULT DETECTION AND CLASSIFICATION: BASIC PRINCIPLE

Voltages and currents are continuously measured at both ends of the DC transmission line. Transient energy is then computed from the measured values of voltages and currents. Signum function of transient energy is then computed, which is used here for fault detection and classification.

Fig. 1 shows the single-line diagram of the monopolar HVDC system used here for the study, where I_M and V_M are the current and voltage measured on the rectifier end (M) of the DC transmission line. Similarly, I_N and V_N are the current and voltage measured at the inverter end (N). The HVDC transmission system used for simulation in this research is established using PSCAD/EMTDC. It is based on the CIGRE benchmark system for the HVDC monopolar configuration [44].

The system is a 500-kV, 1000-MW HVDC link with a monopolar configuration, using 12-pulse converters on both the rectifier and inverter sides. AC source 1 and AC source 2 include supply circuits, transformers, and AC filter banks. The AC filters are installed to absorb the harmonics generated by the converter circuits. They also provide a reactive power supply to the converters. Rectifiers and inverters are modeled using a six-pulse Graetz Bridge circuit. The DC line is modeled using an equivalent T network with smoothing reactors inserted on both sides. DC filters are installed at both ends of the DC transmission line. The DC filter and its design are shown in the Appendix in Fig. 11. The positive direction of the current is assumed, as depicted in the figure.

The transient energies at the two ends of the DC line, evaluated from time 0 to t, are given by

$$\Delta E_M = \int_0^t \Delta P_M(t)\,.dt \tag{1}$$

$$\Delta E_N = \int_0^t \Delta P_N(t)\,.dt \tag{2}$$

where,

ΔE_M = transient energy at rectifier end M
ΔE_N = transient energy at inverter end N
ΔP_M = incremental power at rectifier end M
ΔP_N = incremental power at inverter end N

In discrete form, the above expression of transient energy over one ac power cycle at the rectifier end at any instant j will become

$$\begin{aligned}\Delta EM_j &= \sum_{j=j}^{(j-39)} \Delta P_{Mj}.\Delta t \\ &= \sum_{j=j}^{(j-39)} \Delta V_{Mj}.\Delta I_{Mj}.\Delta t \end{aligned} \quad (3)$$

where,

$$\begin{aligned}\Delta V_{Mj} &= V_{Mj} - V_{M(J-40)} \\ \Delta I_{Mj} &= I_{Mj} - I_{M(j-40)} \\ \Delta t &= \text{sampling interval}\end{aligned}$$

Similarly, for the inverter end N, we have

$$\Delta E_{Nj} = \sum_{j=j}^{(j-39)} \Delta V_{Nj}.\Delta I_{Nj}.\Delta t \quad (4)$$

The signum function of transient energy is then computed for both ends of the transmission line using the below equation [45]:

$$\text{sgn}(\Delta E) = \begin{cases} -1; & \Delta E < 0 \\ 0; & \Delta E = 0 \\ 1; & \Delta E > 0 \end{cases} \quad (5)$$

Finally, the value of summation of the signum functions at two ends of the transmission line (ssgn) is obtained from the given equation:

$$\text{ssgn} = \text{sgn}(\Delta E_M) + \text{sgn}(\Delta E_N) \quad (6)$$

The signum functions for E_M and E_N will be zero if no faults occur in the HVDC system. However, if an internal DC fault occurs, the signum functions of E_M and E_N will produce values with non-zero magnitude and opposite signs. If an external AC fault occurs in the HVDC system, E_M and E_N will have values with non-zero magnitude but the same sign. In this case, the signum functions of both components will be either $+1$ or -1, resulting in a sum of the signum functions (ssgn) value of either $+2$ or -2, respectively. On the other hand, when there is no external AC fault and no faults in the HVDC system, one of the components will have a signum function of $+1$, and the other will have a signum function of -1. Consequently, the obtained value of the sum of their signum functions (ssgn) will have a zero value.

III. FAULT CLASSIFICATION ALGORITHM

Fig. 2 illustrates the algorithm for detecting and categorizing faults according to the abovementioned principle.

Voltages and currents are continuously monitored synchronously at both the terminal ends of the DC transmission line to monitor HVDC system faults. Based on the measured values, incremental voltage, incremental current, and transient energy are calculated.

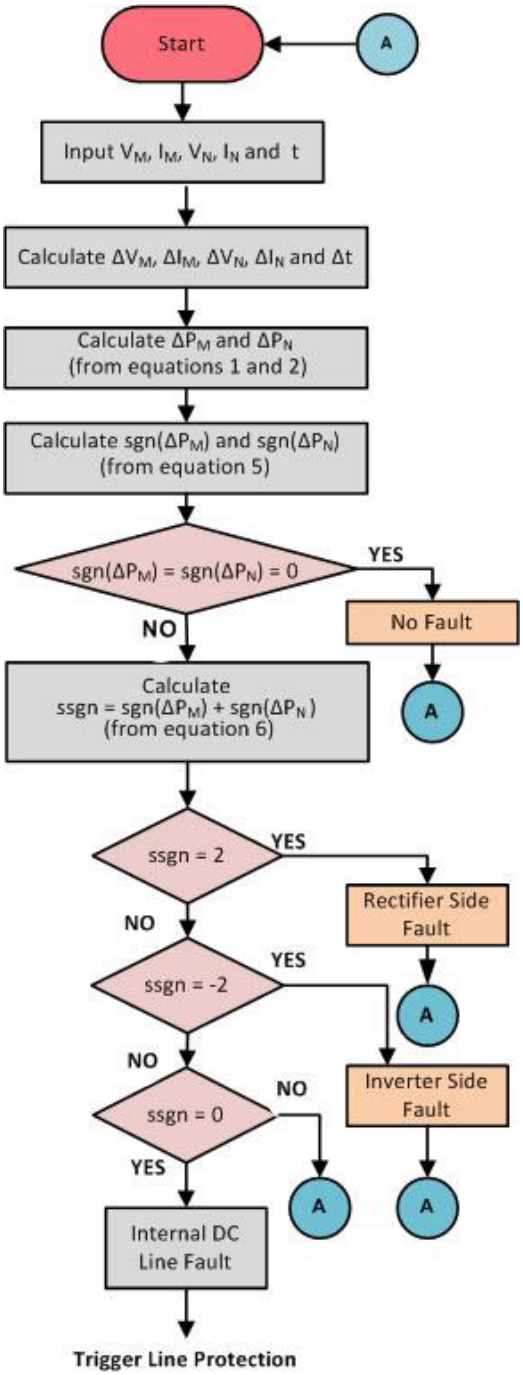

FIGURE 2. Fault Classification Algorithm.

The signum function of the transient energy is then determined at each end. If the signum functions computed at both ends, ΔE_M and ΔE_N, are zero, the system has no faults. In such cases, taking the next set of voltage and current samples is repeated.

However, if this condition is violated, the value of (ssgn) is further computed for fault classification. Subsequently, appropriate measures are taken as mentioned below:

TABLE 1. System specifications.

Specification	Value
Voltage of the AC source at the rectifier side	345 kV
frequency of AC source at rectifier side	50 Hz
voltage of the AC source at the inverter side	230 kV
frequency of AC source at inverter side	50 Hz
DC transmission line voltage rating	500 kV
DC transmission line length	800 km
DC transmission line current	2 kA
power of DC transmission line	1000 MW

a. If ssgn = 2, ac fault at the rectifier side is detected, the program returns to collect the subsequent samples.
b. If ssgn = −2, ac fault at the inverter-side is detected, the program returns to collect the subsequent samples.
c. If ssgn = ± 1, the program returns to collect the next set of samples.
d. If ssgn = 0, fault in a DC transmission line is indicated.

It is a common practice to confirm the existence of an internal fault for one or two samples for security purposes. It would be better to verify the presence of an internal fault for two consecutive samples and thus introduce a waiting time of 1 ms before triggering the line protection.

IV. SIMULATION AND SIMULATION RESULTS

The performance of the proposed algorithm is evaluated on the proposed test system. Simulation is done using EMTDC/PSCAD software. The following two subsections give details of the simulation and the simulation results.

A. SIMULATION DETAILS

Values of various parameters of the monopolar HVDC system selected are shown in Table 1. The DC transmission line is modeled as a distributed parameter system. The HVDC system includes DC filters placed on the two line ends, which are not shown in Fig. 1. However, the Appendix provides the configuration of the DC filter at each end as well as the values of its parameters. Voltage and current at the two ends were sampled at 2 kHz.

The system has been simulated for five different fault locations along the system, as shown in Fig. 1. A line-to-ground fault was created on the DC line at the sending end (DF_1), at the mid-point (DF_2) and the receiving end (DF_3). A 3-phase fault was created on the AC side of the rectifier (RF) and the AC side of the inverter (IF). For each fault location, the test system was simulated for five fault resistance values (R_F), viz., 0, 10, 100, 1000, and 2000 ohms. Fault has been created at 0.5 sec in each case study.

B. RESULTS OF SIMULATION

The simulation results carried out as above are presented below under paragraphs (1 to 5).

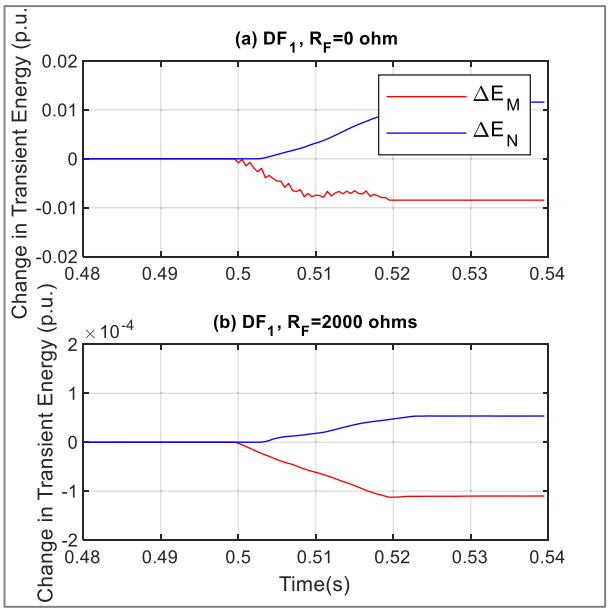

FIGURE 3. System response for DF_1 (a) R_F = 0 ohms and (b) R_F = 2000 ohms.

1) RESULTS OF SIMULATION FOR DC FAULT AT THE SENDING END (DF_1)

Fig. 3 presents incremental transient energy curves over 20 ms before and 40 ms after the instant of fault occurrence (0.5 s) for internal fault near the sending end (DF_1). The response is shown only for the lowest and highest values of fault resistance, as the response is nearly the same for all values.

As observed from Fig. 3 (a), the incremental transient energy at terminal end M remains negative and that at terminal end N positive for a minimum of two AC power cycles after the occurrence of fault with R_F = 0 ohm. Fig. 3 (b) shows a similar curve pattern for R_F = 2000 ohms.

2) RESULTS OF SIMULATION FOR DC FAULT AT THE MID-POINT (DF_2)

Fig. 4 shows the system response curves for the internal fault at the mid-point of the line (DF_2). The nature of the response is very similar to that for DF_1.

3) RESULTS OF SIMULATION FOR DC FAULT AT THE RECEIVING END (DF_3)

Fig. 5 shows the system response curves for the internal fault at the receiving end of the line (DF_3). The nature of the response is very similar to that for DF_1 and DF_2.

4) RESULTS OF SIMULATION FOR AC FAULT AT THE RECTIFIER SIDE (RF)

Response curves for the external fault near rectifier (RF) for all five values of fault resistance are shown in Fig. 6. As the fault resistance value increases, the magnitude of the incremental transient energy reduces. The scale on the axis has been progressively amplified in these figures to amplify

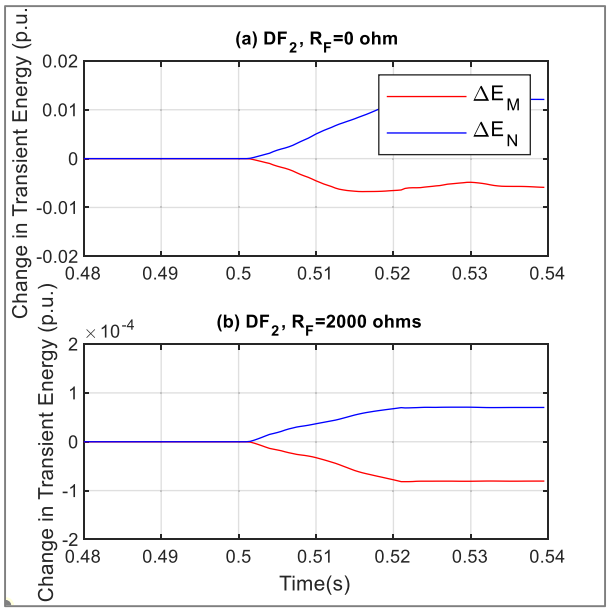

FIGURE 4. System response for DF_2 (a) $R_F = 0$ ohms, (b) $R_F = 2000$ ohms.

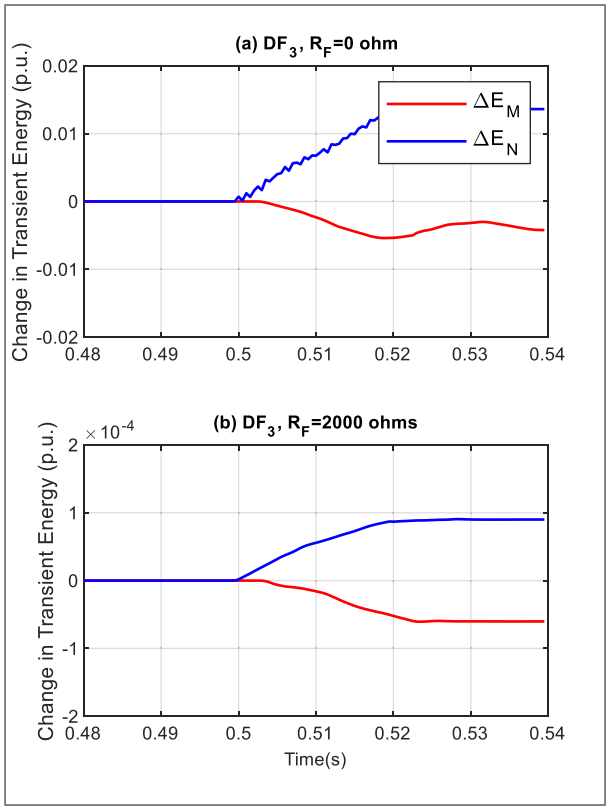

FIGURE 5. System response for DF_3 (a) $R_F = 0$ ohms and (b) $R_F = 2000$ ohms.

the changes. The incremental transient energy at both ends of the line is positive for all fault resistance values.

5) RESULTS OF SIMULATION FOR AC FAULT AT THE INVERTER SIDE (IF)

The response curves for the external fault at the inverter side (IF) for the five values of fault resistance are shown in Fig. 7.

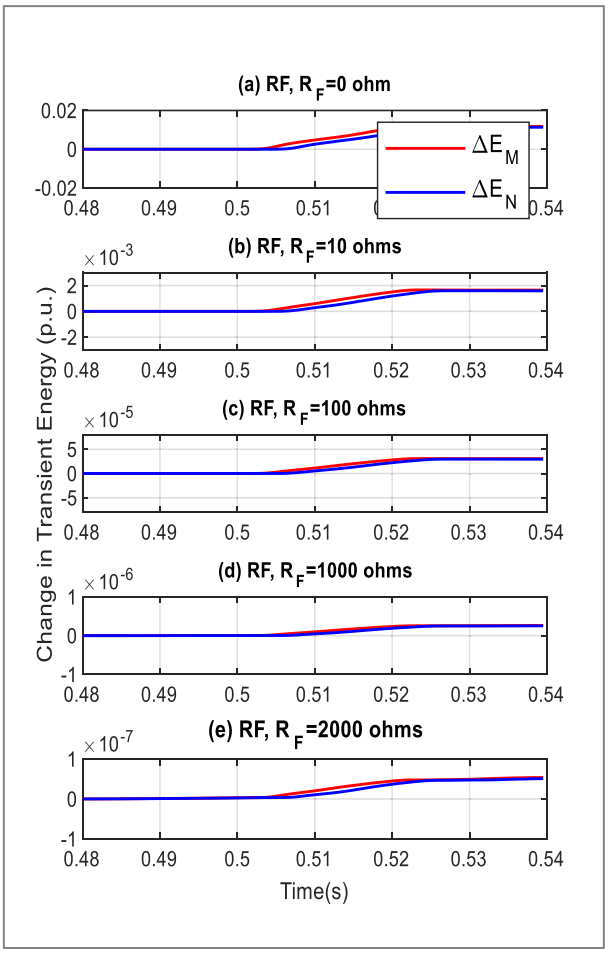

FIGURE 6. System response for RF (a) $R_F = 0$ ohms, (b) $R_F = 10$ ohms, (c) $R_F = 100$ ohms, (d) $R_F = 1000$ ohms, (e) $R_F = 2000$ ohms.

It is seen that the incremental transient energy at both ends for 0, 10, and 100 ohms of fault resistance is negative. In contrast, the same is positive for 1000 and 2000 ohms values. Moreover, the absolute value of the incremental transient energy reduces as the fault resistance increases.

V. EVALUATION OF FAULT CLASSIFICATION ALGORITHM

The simulation output described in this section is utilized as input samples for the protection algorithm outlined in Section III. This algorithm calculates the signum function of the transient energy variance at both ends and their sum for each specified fault location and resistance value. These signum functions are the basis on which the algorithm classifies the fault. The algorithm's performance is covered in detail in subsections A through C and is summarized in subsection D below:

A. ALGORITHM PERFORMANCE ON INTERNAL FAULTS (DF_1, DF_2, AND DF_3)

The algorithm's performance, in terms of success and time of classification, for any single fault location was found to be the same for all values of fault resistance. Therefore, only one set of results is given in Fig. 8 for each internal fault

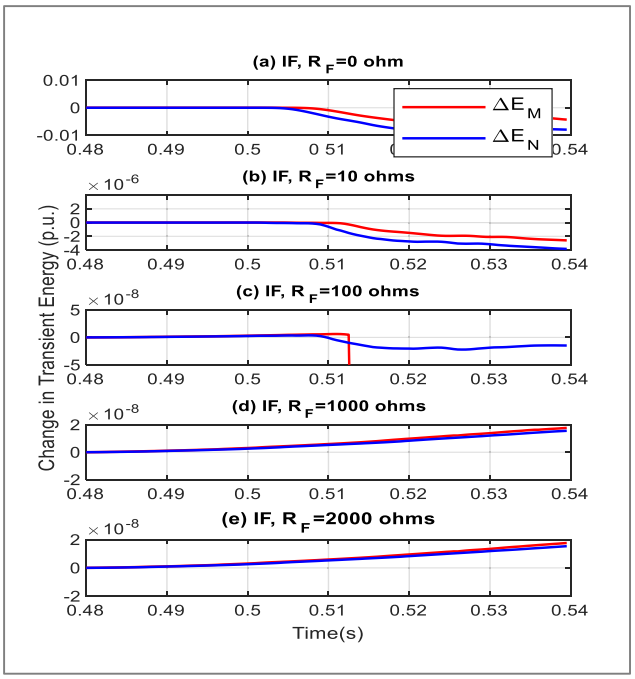

FIGURE 7. System response for IF (a) $R_F = 0$ ohms, (b) $R_F = 10$ ohms, (c) $R_F = 100$ ohms, (d) $R_F = 1000$ ohms, (e) $R_F = 2000$ ohms.

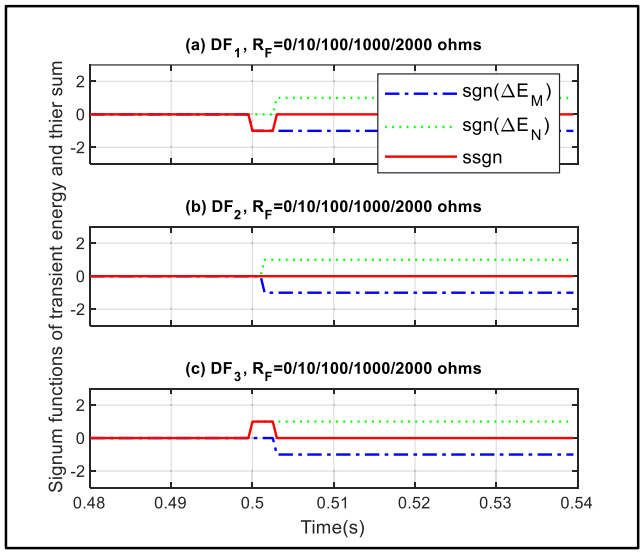

FIGURE 8. Signum functions and their sum for internal faults (a) DF_1, (b) DF_2, and (c) DF_3.

location. As seen from Fig. 8 (a), for sending end dc line fault DF_1, sgn(ΔEM) becomes +1 instantaneously, and sgn (ΔEN) becomes −1 after 3 ms delay, and hence their sum becomes 0 in 3 ms (indicating dc line fault). The classification time in this case is 1.5 ms, as shown for mid-point dc line fault DF_2 in Figure 8(b). Figure 8(c)'s observations for receiving end DC line fault DF_3 show a classification time of 3 ms for DF_3.

The delay of 1.5 ms for DF_2 is due to the time the current and voltage disturbances travel from the fault point (mid-point of the line) to the relay end, which is 400 km away. By the same logic, the delay of 3 ms for DF_1 and DF_3 is due to

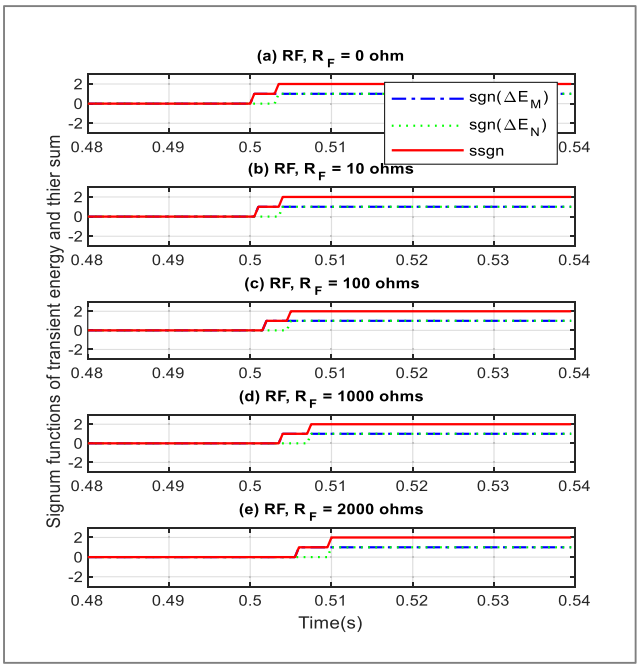

FIGURE 9. Signum functions and their sum for rectifier side external fault.

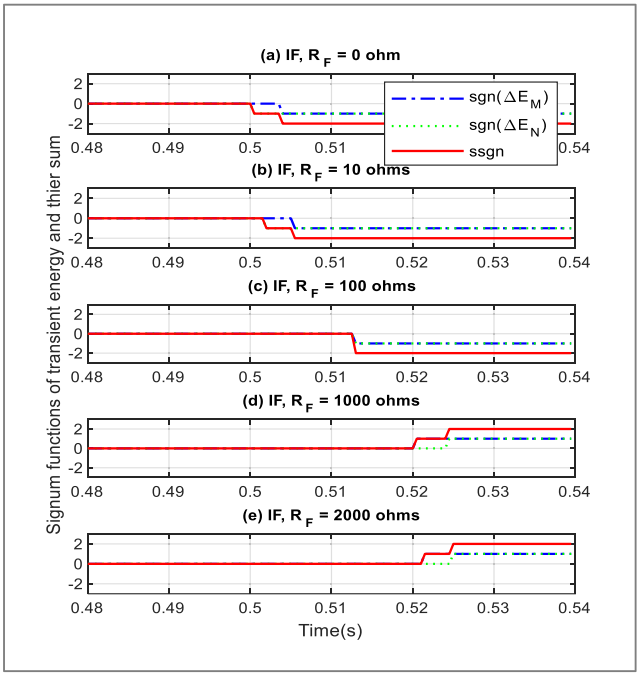

FIGURE 10. Signum functions and their sum for inverter side external fault.

the time taken for the disturbance to travel from the fault point on one end of the line to the relay location at the opposite end of the 800 km long line.

B. ALGORITHM PERFORMANCE FOR RECTIFIER-SIDE EXTERNAL FAULT

Figs. 9 (a) to (e) show that the classification time of the algorithm increases progressively from 3.5 ms for

TABLE 2. Summary of performance of protection system.

Type of Fault	Fault Location	Fault Resistance (ohms)	sgn (ΔE_M)	sgn (ΔE_N)	ssgn	Detection and Classification	Fault Classification time (ms)
No-Fault	-	-	0	0	0	No-Fault	-
Internal Fault (L-G)	DF_1	0-2000	-1	1	0	Internal Fault	3
	DF_2	0-2000	-1	1	0	Internal Fault	1.5
	DF_3	0-2000	-1	1	0	Internal Fault	3
External Fault (L-L-L-G)	Rectifier Fault	0	1	1	2	External Fault	3.5
		10	1	1	2	External Fault	4
		100	1	1	2	External Fault	5
		1000	1	1	2	External Fault	7
		2000	1	1	2	External Fault	10
External Fault (L-L-L-G)	Inverter Fault	0	-1	-1	-2	External Fault	4
		10	-1	-1	-2	External Fault	5.5
		100	-1	-1	-2	External Fault	13
		1000	1	1	2	External Fault	20.5
		2000	1	1	2	External Fault	21.5

TABLE 3. Comparative study of present work with recently reported techniques.

Features	Present Work	Ref [19] Kong et al.	Ref [36] Shu et al.	Ref [46] Gao et al.	Ref [47] Xiadong et al.	Ref [48] Zheng et al.
Operating Time	<=3ms	=>60ms	Not shown	10ms	Not shown	40ms
Sensitivity to fault resistance (R_F)	Insensitive over 0 – 2000 ohms	Insensitive over 0 – 500 ohms (not studied for higher values)	Reduces with an increase in R_F	Not studied	Reduces with an increase in R_F	Reduces with an increase in R_F
Sensitivity to distance from relay	Sensitivity maintained	Sensitivity maintained	Decreases with an increase in distance	Not studied	Not studied	Reduces with an increase in distance

R_F = 0 ohms to 10 ms for R_F = 2000 ohms. However, the algorithm classifies the fault for every value of R_F as an external rectifier-side fault.

C. ALGORITHM PERFORMANCE FOR INVERTER-SIDE EXTERNAL FAULT

As given in Figs. 10 (a) to (e), the classification time for external inverter end faults also increases with an increase in fault resistance value.

The type of fault indicated for low values of fault resistance (R_F = 0 ohms, R_F = 10 ohms, and R_F = 100 ohms), as observed from Figs. 10 (a), (b), and (c), is "external inverter end fault (ssgn = −2". Fig. 10(d) and Fig. 10(e), for R_F = 1000 ohms and 2000 ohms, respectively, show that ssgn = +2, indicating an "external fault" though confusing with rectifier end AC fault. It can be observed that the protection algorithm fails to differentiate between rectifier-side AC fault and inverter-side AC fault for higher values of fault resistance (R_F = 1000 ohms and 2000 ohms). However, it is noted that the classification is still correct as much as the type of fault indicates external fault. Loss of distinction between external inverter end and external rectifier end faults at high values of fault resistance has no consequence because the protection is not triggered in either case.

D. PERFORMANCE SUMMARY

Table 2 summarizes the performance findings of the protection algorithm for all specified values of fault locations and fault resistances. As seen from the last column, the classification time is typically between 1.5 and 3 ms for

all internal faults and all values of fault resistance. This classification time is the time the disturbance wave takes to travel from the fault point to the relay location. As the value of fault resistance rises from 0 ohms to 2000 ohms, the classification time for all external faults gradually increases from 3 ms to 21.5 ms. The detection and fault classification time for the mid-point DC line fault is 1.5 ms, and that for all other fault locations is 3 ms. It can be seen from Table 2 that the sensitivity of the protection algorithm is not affected by the value of fault resistance for DC internal faults. The sum of the signum function (ssgn) is zero for all values of fault resistance ranging from 0 ohms to 2000 ohms.

VI. CONCLUSION

A new technique and protection algorithm have been successfully developed and presented for fault detection and classification in monopolar HVDC transmission systems. These are entirely based on the signum function values of the transient energy variation at the DC transmission line's two ends. The total sum of the signum functions, along with the individual value of signum functions, is used to classify different faults and the no-fault condition. A comprehensive evaluation of the technique and algorithm has been done by simulating other fault conditions on a monopolar HVDC system. DC line-to-ground faults were simulated near the line's terminals and at its mid-point as internal faults, and three-phase AC faults at the rectifier and inverter sides as external faults. Five values of fault resistance varying from 0 ohms to 2000 ohms were used for each fault location.

The proposed algorithm's performance can be summarized as follows:

i. Without fail, the algorithm can categorize no-fault, internal, and external faults.

ii. All internal faults are detected and classified in 1.5 to 3 ms depending on the location of the fault, irrespective of fault resistance values.

iii. Rectifier and inverter side AC faults are classified in 3 to 21.5 ms depending on the value of fault resistance (classification time increasing with an increase in fault resistance values).

A comparative study of the performance of the proposed technique with the techniques reported in the literature and reviewed in this paper is presented in Table 3.

The comparison concerns the operating time, sensitivity to the value of fault resistance, and the effect of fault distance from the relay location on the sensitivity. It is concluded that the proposed technique/algorithm is (a) fastest in detecting internal faults, (b) insensitive to fault resistance values, and (c) unaffected by the distance of fault from the relay location.

According to continuing research, a real-time protection strategy using Field Programmable Gate Arrays (FPGA) may be built. Then, the suggested protection method will be a useful advancement in the field of HVDC protection.

APPENDIX

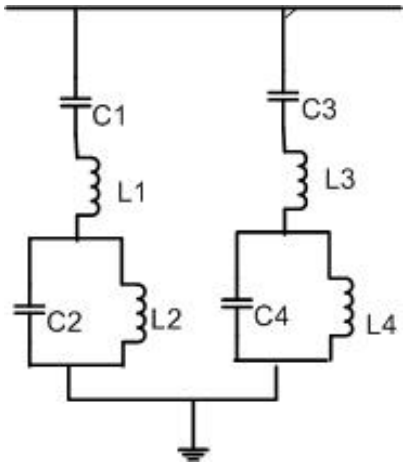

FIGURE 11. Configuration of DC filter.

$L1 = 0.01171H, C1 = 2\mu F$
$L2 = 0.005874H, C2 = 9.074\mu F$
$L3 = 0.00646H, C3{=}2\ \mu F$
$L4 = 0.01135H, C4{=}3.752\ \mu F$

REFERENCES

[1] B. R. Anderson and X. Lie, "Hybrid HVDC system for power transmission to island networks," *IEEE Trans. Power Del.*, vol. 19, no. 4, pp. 1884–1890, Oct. 2004, doi: http://10.1109/TPWRD.2004.835031.

[2] J.O. Reilly, A.R. Wood, and C.M. Osauskas, "Frequency domain based control design for an HVDC converter connected to a weak AC network," *IEEE Trans. Power Del.*, vol. PWRD-3, no. 4, pp. 2064–2071, Oct. 1988, doi: http://10.1109/TPWRD.2003.813638.

[3] D. Wang, D. Yu, H. Yang, and M. Hou, "Novel travelling wave directional pilot protection for VSC-HVDC transmission line," *IET Gener., Transmiss. Distrib.*, vol. 14, no. 9, pp. 1705–1713, May 2020, doi: http://10.1049/iet-gtd.2019.0394.

[4] S. Sambhi, H. Sharma, V. Bhadoria, P. Kumar, R. Chaurasia, G. Fotis, V. Vita, L. Ekonomou, and C. Pavlatos, "Economic feasibility of a renewable integrated hybrid power generation system for a rural village of Ladakh," *Energies*, vol. 15, no. 2, p. 9126, Dec. 2022, doi: https://doi.org/10.3390/en15239126.

[5] T. I. Maris, S. Kourtesi, L. Ekonomou, and G. Fotis, "Modeling of a single-phase photovoltaic inverter," *Sol. Energy Mater. Sol. Cells*, vol. 91, no. 18, pp. 1713–1725, Nov. 2007, doi: https://doi.org/10.1016/j.solmat.2007.05.027.

[6] G. Fotis, C. Dikeakos, E. Zafeiropoulos, S. Pappas, and V. Vita, "Scalability and replicability for smart grid innovation projects and the improvement of renewable energy sources exploitation: The FLEXITRANSTORE case," *Energies*, vol. 15, no. 13, p. 4519, Jun. 2022, doi: https://doi.org/10.3390/en15134519.

[7] W. Long and S. Nilsson, "HVDC transmission: Yesterday and today," *IEEE Power Energy Mag.*, vol. 5, no. 2, pp. 22–31, Mar./Apr. 2007, doi: https://10.1109/MPAE.2007.329175.

[8] M. Muniappan, "A comprehensive review of DC fault protection methods in HVDC transmission systems," *Protection and Control Mod. Power Syst.*, vol. 6, no. 1, pp. 1–19, Dec. 2021, doi: https://10.1186/s41601-020-00173-9.

[9] S. Lei, H. Shu, Z. Li, and Y. Dai, "A faulty pole detection method for the VSC-HVDC system based on the aperiodic component energy," *Electr. Power Syst. Res.*, vol. 212, no. 8, Nov. 2022, Art. no. 108650, doi: https://10.1016/j.epsr.2022.108650.

[10] H. Kunlun, C. Zexiang, and L. Yang, "Study on protective performance of HVDC transmission line protection with different types of line fault," in *Proc. 4th Int. Conf. Electr. Utility Deregulation Restructuring Power Technol. (DRPT)*, Jul. 2011, pp. 358–361, doi: 10.1109/DRPT.2011.5993917.

[11] A. Li, Z. Cai, Q. Sun, X. Li, D. Ren, and Z. Yang, "Study on the dynamic performance characteristics of HVDC control and protections for the HVDC line fault," in *Proc. IEEE Power Energy Soc. Gen. Meeting*, Jul. 2009, pp. 1–5, doi: https://10.1109/PES.2009.5275974.

[12] F. Mohammad, "Detection and classification of internal faults in bipolar HVDC transmission lines based on K-means data description method," *Int. J. Elect. Power Energy Syst.*, vol. 104, pp. 615–625, Jan. 2019, doi: https://doi.org/10.1016/j.ijepes.2018.07.044.

[13] J. Zheng, M. Wen, Y. Chen, and X. Shao, "A novel differential protection scheme for HVDC transmission lines," *Int. J. Electr. Power Energy Syst.*, vol. 94, pp. 171–178, Jan. 2018, doi: 10.1016/j.ijepes.2017.07.006.

[14] S. Kang and C. Hwang, "Current-restrained DC under-voltage protection for a bipolar HVDC system," *J. Eng.*, vol. 2018, no. 15, pp. 944–949, Sep. 2018, doi: http://10.1049/joe.2018.0279.

[15] Y. Li, Y. Zhang, J. Song, L. Zeng, and J. Zhang, "A novel pilot protection scheme for LCC-HVDC transmission lines based on smoothing-reactor voltage," *Electr. Power Syst. Res.*, vol. 168, pp. 261–268, Mar. 2019, doi: 10.1016/j.epsr.2018.12.012.

[16] R. Li, L. Xu, and L. Yao, "DC fault detection and location in meshed multiterminal HVDC systems based on DC reactor voltage change rate," *IEEE Trans. Power Del.*, vol. 32, no. 3, pp. 1516–1526, Jun. 2017, doi: 10.1109/TPWRD.2016.2590501.

[17] Y. Li, Y. Gong, and B. Jiang, "A novel traveling-wave-based directional protection scheme for MTDC grid with inductive DC terminal," *Electr. Power Syst. Res.*, vol. 157, pp. 83–92, Apr. 2018, doi: https://10.1016/j.epsr.2017.12.010.

[18] S. Luo, X. Dong, S. Shi, and B. Wang, "A directional protection scheme for HVDC transmission lines based on reactive energy," *IEEE Trans. Power Del.*, vol. 31, no. 2, pp. 559–567, Apr. 2016, doi: 10.1109/TPWRD.2015.2461450. http://10.1109/PESGM.2016.7741135.

[19] F. Kong, Z. Hao, and B. Zhang, "Improved differential current protection scheme for CSC-HVDC transmission lines," *IET Gener., Transmiss. Distrib.*, vol. 11, no. 4, pp. 978–986, Mar. 2017, doi: https://doi.org/10.1049/iet-gtd.2016.0995.

[20] S. Gao, Q. Liu, and G.B. Song, "Current differential protection principle of HVDC transmission system," *IET Gener., Transmiss. Distrib.*, vol. 11, no. 5, pp. 1286–1292, Jan. 2017, doi: https://doi.org/10.1049/iet-gtd.2016.1380.

[21] Y. Zhang, Y. Li, J. Song, B. Li, and X. Chen, "A new protection scheme for HVDC transmission lines based on the specific frequency current of DC filter," *IEEE Trans. Power Del.*, vol. 34, no. 2, pp. 420–429, Apr. 2019, doi: 10.1109/TPWRD.2018.2867737. https://10.1109/TPWRD.2018.2867737.

[22] X. Chu, "Unbalanced current analysis and novel differential protection for HVDC transmission lines based on the distributed parameter model," *Electr. Power Syst. Res.*, vol. 171, pp. 105–115, Jun. 2019, doi: 10.1016/j.epsr.2019.02.003.

[23] X. Chu, "Transient numerical calculation and differential protection algorithm for HVDC transmission lines based on a frequency-dependent parameter model," *Int. J. Elect. Power Energy Syst.*, vol. 108, pp. 107–116, Jun. 2019, doi: https://10.1016/j.ijepes.2018.12.039.

[24] A. Saber, H. Zeineldin, T. El-Fouly, and A. Al-Durra, "Current differential relay characteristic for bipolar HVDC transmission line fault detection," *IET Gener., Transmiss. Distrib.*, vol. 14, no. 23, pp. 5505–5513, Dec. 2020, doi: https://doi.org/10.1049/iet-gtd.2020.0556.

[25] M.M. Kooshki, S. S. Mirhosseini, and S. Jamali, "Single-end protection algorithm for HVDC transmission lines based on the current difference," *IET Gener., Transmiss. Distrib.*, vol. 14, no. 20, pp. 4339–4351, Jul. 2020, doi: https://doi.org/10.1049/iet-gtd.2019.1621.

[26] Y. Zhang, Y. Li, J. Song, X. Chen, Y. Lu, and W. Wang, "Pearson correlation coefficient of current derivatives based pilot protection scheme for long-distance LCC-HVDC transmission lines," in *Proc. IEEE 8th Int. Conf. Adv. Power Syst. Autom. Protection (APAP)*, Oct. 2019, pp. 1367–1371, doi: 10.1109/APAP47170.2019.9224937.

[27] J. Duan, H. Li, Y. Lei, and L. Tuo, "A novel non-unit transient based boundary protection for HVDC transmission lines using synchrosqueezing wavelet transform," *Int. J. Elect. Power Energy Syst.*, vol. 115, Feb. 2020, Art. no. 105478, doi: https://doi.org/10.1016/j.ijepes.2019.105478.

[28] D. Wang, M. Hou, M. Gao, and F. Qiao, "Travelling wave directional pilot protection for hybrid LCC-MMC-HVDC transmission line," *Int. J. Electr. Power Energy Syst.*, vol. 115, Feb. 2020, Art. no. 105431, doi: 10.1016/j.ijepes.2019.105431.

[29] H. Cao, M. Xie, Z. Zhou, X. Wang, B. Yu, D. Du, H. Wang, T. Wang, and Y. Yu, "A pilot protection scheme for UHVDC lines based on backward traveling-wave difference," in *Proc. IEEE 8th Int. Conf. Adv. Power Syst. Autom. Protection (APAP)*, Oct. 2019, pp. 85–90, doi: 10.1109/APAP47170.2019.9224770.

[30] S. Ankar and A. Yadav, "A high-speed protection strategy for bipolar CSC-Based HVDC transmission system," *Electr. Power Compon. Syst.*, vol. 49, pp. 48–66, Jun. 2021, doi: https://10.1080/15325008.2021.1937397.

[31] J. Ma, J. Kang, Y. Zhou, Y. Wu, and P. Cheng, "A new pilot directional protection method for HVDC line based on the polarity of inductive energy," *IET Gener., Transmiss. Distrib.*, vol. 15, no. 22, pp. 3215–3228, Jul. 2021, doi: https://doi.org/10.1049/gtd2.12253.

[32] N. Liu, Y. Li, S. Li, T. Li, and L. Yu, "A pilot protection for LCC-HVDC transmission lines based on measured surge impedance at tuning frequency," *IEEE Trans. Power Del.*, vol. 37, no. 3, pp. 2090–2103, Jun. 2022, doi: 10.1109/TPWRD.2021.3103913. https://10.1109/TPWRD.2021.3103913.

[33] J. Ma, Y. Wu, C. Liu., and A. G. Phadke, "A pilot protection for HVDC transmission lines based on current correlation," in *Proc. IEEE 4th Int. Elect. Energy Conf. (CIEEC)*, Wuhan, China, May 2021, pp. 1–6, doi: https://10.1109/CIEEC50170.2021.9510742.

[34] D. Zhang, C. Wu, J. He, and C. Liang, "A new protection scheme for transmission line of three-terminal hybrid HVDC system," *Int. J. Elect. Power Energy Syst.*, vol. 134, Jan. 2022, Art. no. 107446, doi: https://doi.org/10.1016/j.ijepes.2021.107446.

[35] S. Lei, H. Shu, and Z. Li, "A protection principle of LCC-VSC three-terminal HVdc system based on instantaneous boundary impedance," *IEEE Trans. Ind. Electron.*, pp. 1–10, Mar. 2023, doi: 10.1109/TIE.2023.3260339. https://10.1109/TIE.2023.3260339.

[36] H. Shu, S. Wang, and S. Lei, "Single-ended protection method for hybrid HVDC transmission line based on transient voltage characteristic frequency band," *Protection Control Mod. Power Syst.*, vol. 8, no. 26, pp. 1–11, Jun. 2023, doi: https://10.1186/s41601-023-00301-1.

[37] B. Wang, L. Yang, and X. Dong, "Fault location method for high-voltage direct current transmission line using incident current travelling waves," *J. Eng.*, vol. 15, pp. 1165–1168, Sep. 2018, doi: https://doi.org/10.1049/joe.2018.0278.

[38] D. Wang, M. Hou, M. Gao, and F. Qiao, "Travelling wave directional pilot protection for hybrid HVDC transmission line," *Int. J. Elect. Power Energy Syst.*, vol. 107, pp. 615–627, May 2019, doi: https://doi.org/10.1016/j.ijepes.2018.12.028.

[39] X. Liu, A. H. Osman, and O. P. Malik, "Hybrid traveling wave/boundary protection for bipolar HCDC line," in *IEEE Power Energy Soc. Gen. Meeting*, Beijing, China, Jul. 2009, pp. 1–8, doi: https://doi.org/10.1109/PES.2009.5276029.

[40] C. Zhang, G. Song, T. Wang, L. Wu, and L. Yang, "Non-unit traveling wave protection of HVDC grids using Levenberg–Marquart optimal approximation," *IEEE Trans. Power Del.*, vol. 35, no. 5, pp. 2260–2271, Oct. 2020, doi: 10.1109/TPWRD.2020.2964717. https://doi.org/10.1109/TPWRD.2020.2964717.

[41] C. Li, A. M. Gole, and C. Zhao, "A fast DC fault detection method using DC reactor voltages in HVDC grids," *IEEE Trans. Power Del.*, vol. 33, no. 5, pp. 2254–2264, Apr. 2018, doi: https://10.1109/TPWRD.2018.2825779.

[42] D. Tzelepis, A. Dysko, G. Fusiek, J. Nelson, P. Niewczas, D. Vozikis, P. Orr, N. Gordon, and C. D. Booth, "Single-ended differential protection in MTDC networks using optical sensors," *IEEE Trans. Power Del.*, vol. 32, no. 3, pp. 1605–1615, Jun. 2017, doi: 10.1109/TPWRD.2016.2645231. https://10.1109/TPWRD.2016.2645231.

[43] T. Lan, H. Xiao, Y. Li, and J. Chen, "Enhanced current differential protection for HVDC grid based on bergeron model: A parameter error tolerable solution," *IEEE Trans. Power Del.*, vol. 36, no. 3, pp. 1869–1881, Jun. 2021, doi: 10.1109/TPWRD.2020.3016730. https://10.1109/TPWRD.2020.3016730.

[44] M. O. Faruque, Y. Zhang, and V. Dinavahi, "Detailed modeling of CIGRE HVDC benchmark system using PSCAD/EMTDC and PSB/SIMULINK," *IEEE Trans. Power Del.*, vol. 21, no. 1, pp. 378–387, Jan. 2006, doi: https://10.1109/TPWRD.2005.852376.

[45] P. Dutta, A. Esmaeilian, and M. Kezunovic, "Transmission-line fault analysis using synchronized sampling," *IEEE Trans. Power Del.*, vol. 29, no. 2, pp. 942–950, Apr. 2014, doi: 10.1109/TPWRD.2013.2296788. https://10.1109/TPWRD.2013.2296788.

[46] S. Gao, G. Song, Z. Ma, and X. Jin, "Novel pilot protection principle for high-voltage direct current transmission lines based on fault component current characteristics," *IET Gener., Transmiss. Distrib.*, vol. 9, no. 5, pp. 468–474, Apr. 2015, doi: https://doi.org/10.1049/iet-gtd.2014.0313.
[47] Z. Zheng, T. Tai, J. S. Thorp, and Y. Yang, "A transient harmonic current protection scheme for HVDC transmission line," *IEEE Trans. Power Del.*, vol. 27, no. 4, pp. 2278–2285, Oct. 2012, doi: 10.1109/TPWRD.2012.2201509. https://10.1109/TPWRD.2012.2201509.
[48] X. Zheng, T. Nengling, Y. Guangliang, and D. Haoyin, "A transient protection scheme for HVDC transmission line," *IEEE Trans. Power Del.*, vol. 27, no. 2, pp. 718–724, Apr. 2012, doi: 10.1109/TPWRD.2011.2179321.

SOMA DEB (Member, IEEE) received the B.Tech. degree in electrical engineering from KNIT, Sultanpur, India, in 2004, the M.Tech. degree in instrumentation and control from NSIT, New Delhi, India, in 2011, and the Ph.D. degree in power systems from Sharda University, Greater Noida, Uttar Pradesh, India, in 2022. She is currently an Assistant Professor with the Department of Electrical Electronics and Communication Engineering, Sharda University. Her research interests include protecting HVDC systems, HVAC lines, and renewable energy systems.

SUMAN LATA (Member, IEEE) received the Bachelor of Engineering degree in instrumentation, the master's degree in technology in electrical and electronics, and the Ph.D. degree, in 2021. She is currently an Electrical Electronics and Communication Engineering Associate Professor (EECE) with Sharda University, Greater Noida, India. She has an experience of almost 22 years in research and academics. She has 32 research articles to her credit. She has been a reviewer at many reputed conferences.

VIKAS SINGH BHADORIA received the B.E. and M.E. degrees in electrical and electronics engineering from RGPV, Bhopal, India, in 2005 and 2009, respectively, and the Ph.D. degree in power systems from Gautam Buddha University, Greater Noida, Uttar Pradesh, India, in 2018. He is currently the Deputy Training and Placement Officer with Shri Vishwakarma Skill University, Palwal, Haryana. His research interests include power system planning, power system reliability, and power system restructuring.

SHUBHAM TIWARI received the B.Tech., M.Tech., and Ph.D. degrees from AKTU, Lucknow. He has published 16 international research articles, one book, and one patent. He has also been granted an Indian patent. His research interests include economic operations in power systems, the modeling of renewable generation, and battery energy storage systems.

THEODOROS I. MARIS received the Diploma degree in electrical engineering and the Ph.D. degree from the School of Engineering, University of Patras, Greece, in 1984 and 1994, respectively. He is currently a Professor with the Control Systems and Industrial Automation Laboratory, National and Kapodistrian University of Athens. His research interests include electric energy systems, direct current interconnections, high voltage direct current converters, electrical drives, photovoltaic inverters, transmission and distribution lines, and artificial neural networks.

VASILIKI VITA received the Bachelor of Engineering degree in electrical engineering from the Higher School of Pedagogical and Technical Education (ASETEM/SELETE), Greece, in 2000, the Master of Science degree in control systems from The University of Sheffield, U.K., in 2002, the Master of Science degree in fundamental and applied cognitive science from the National and Kapodistrian University of Athens, Greece, in 2015, and the Ph.D. degree in electrical engineering from the City University of London, U.K., in 2016. Her research interests include transmission and distribution grids, distributed generation, optimization, lightning performance, electric vehicles, and artificial intelligence. She is the author of more than 90 papers in international journals and conferences.

GEORGIOS FOTIS received the Diploma and Ph.D. degrees in electrical engineering from the National Technical University of Athens, in 2001 and 2006, respectively. From 2006 to 2008, he was a Research Assistant with the NTUA's High Voltage Laboratory and a Lecturer (fixed term), teaching high voltages. He has been an Independent Power Transmission Operator (IPTO), since 2009, working with the Transmission System Operation and Control Department. He has also been an Assistant Professor (fixed term) with the Department of Electrical and Electronics Engineering Educators, School of Pedagogical and Technological Education (ASPETE), teaching electric power systems and high voltages, since 2010. His research interests include power systems, renewable energy sources, transmission and distribution grids, high voltages, electromagnetic compatibility, and electrostatic discharge. He is the author of one book and more than 70 papers in international journals and conferences.